

# Universality of Pattern Formation

Leandro Medina<sup>1,\*</sup> Michael C. Ogilvie<sup>1,†</sup> Moses A. Schindler<sup>1,‡</sup> and Stella T. Schindler<sup>2§</sup>

<sup>1</sup>*Physics Department, Washington University, St. Louis, MO 63130*

<sup>2</sup>*Center for Theoretical Physics, MIT, Cambridge, MA 02139*

## Abstract

We develop a theory of pattern formation in non-Hermitian scalar field theories. Patterned configurations show enhanced Fourier modes, reflecting a tachyonic instability. Multicomponent  $\mathcal{PT}$ -symmetric field theories with such instabilities represent a new universal class of pattern-forming models. The presence of slow modes and long-lived metastable behavior suggests a connection between the computational complexity of the sign problem and the physical characterization of equilibrium phases. Our results suggest that patterning may occur near the critical endpoint of finite density QCD.

arXiv:1906.07288v1 [hep-lat] 17 Jun 2019

## INTRODUCTION

Pattern formation is a ubiquitous phenomenon throughout physics [1–3]. In pattern-forming systems, equilibrium phases exhibit complicated behaviors characterized by persistent inhomogeneous patterns such as stripes and dots. Conventional scalar field theories typically satisfy reflection positivity and thus have positive, self-adjoint transfer matrices [4]; such theories cannot display the modulated behavior associated with patterning. We show that multicomponent  $\mathcal{PT}$ -symmetric scalar field theories with complex actions are a large, natural class of local field theories exhibiting patterning.

$\mathcal{PT}$ -symmetric field theories are invariant under the combined action of a discrete linear transformation  $\mathcal{P}$  and complex conjugation  $\mathcal{T}$  [5, 6]. This symmetry implies that each eigenvalue of the transfer matrix is either real or part of a complex conjugate pair. It is this latter possibility that is responsible for modulated behavior and pattern formation. The prototypical example of a  $\mathcal{PT}$ -symmetric field theory is the  $i\phi^3$  model, which is the field theory for the Lee-Yang transition [7]. In this case  $\mathcal{P}$  takes  $\phi \rightarrow -\phi$ . Many  $\mathcal{PT}$ -symmetric models, including the  $i\phi^3$  model, have complex actions and therefore suffer from the sign problem [8]. QCD at nonzero chemical potential is of great interest in nuclear and particle physics but has a sign problem that has severely hampered its study [9, 10].

In this paper we consider a  $\mathcal{PT}$ -symmetric field theory that can be studied both analytically and with lattice simulations. Extensive simulations of this model indicate a smooth transition between pattern morphologies, in contrast to microphase behavior [2, 11], which assumes clear distinctions between different morphologies. Instead we find a unifying principle: tachyonic instabilities drive pattern formation. We analytically derive a criterion describing when homogeneous phases are unstable to patterning. The pattern-forming region of parameter space exhibits increased computational complexity characterized by slow modes and long autocorrelation times in simulations. This suggests a connection between the computational difficulty associated with the sign problem and the physical characterization of equilibrium phases in scalar field theories.

A recent development in lattice simulations allows us to simulate the complex action

$$S(\phi, \chi) = \sum_x \frac{1}{2}(\partial_\mu \phi)^2 + \frac{1}{2}(\partial_\mu \chi)^2 + V(\phi, \chi), \quad (1)$$

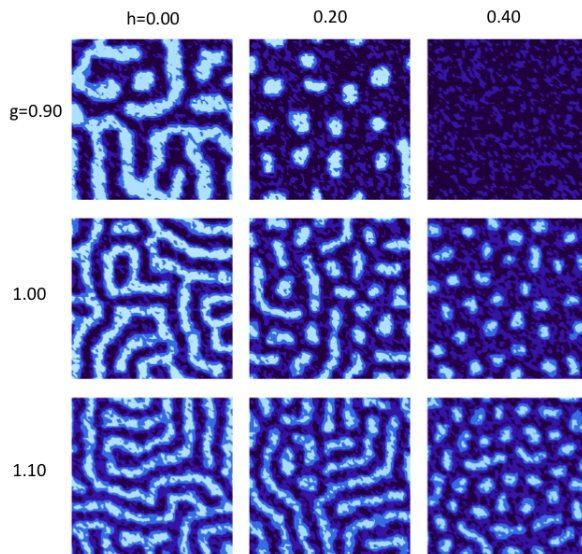


FIG. 1. (color online) Configuration snapshots of  $\phi$  in Eq. (3) on a  $64^2$  lattice for several values of  $h$  and  $g$ . The color scale runs from  $-3$  to  $3$ , ranging from dark to light. From left to right,  $h = 0.0, 0.2$ , and  $0.4$ ; from top to bottom:  $g = 0.9, 1.0$ , and  $1.1$ . The other parameters are  $m_\chi^2 = 0.5$ ,  $\lambda = 0.1$ , and  $v = 3$ . Each configuration was obtained after a hot start followed 20,000 sweeps through the lattice.

where we set

$$V(\phi, \chi) = \frac{1}{2}m_\chi^2\chi^2 - ig\phi\chi + \lambda(\phi^2 - v^2)^2 + h\phi. \quad (2)$$

Eq. (1) represents a Hermitian scalar field  $\phi(x)$  coupled to a  $\mathcal{PT}$ -symmetric scalar field  $\chi(x)$  by the imaginary strength  $ig$ . The dual action of Eq. (1) takes the form

$$\tilde{S} = \sum_x \frac{1}{2}[\partial_\mu\phi(x)]^2 + \frac{1}{2}\pi_\mu^2(x) + \tilde{V}[\phi(x), \partial \cdot \pi(x)], \quad (3)$$

where the dual potential  $\tilde{V}$  is given by  $\tilde{V}(\phi, \partial \cdot \pi) = (\partial \cdot \pi - g\phi)^2/2m_\chi^2 + \lambda(\phi^2 - v^2)^2 + h\phi$ . This model was recently studied for the case  $h = 0$  in two and three dimensions [12]. Here we extend the study of this model to the full  $g-h$  plane. We present extensive simulations in  $d = 2$ , in which we vary the parameters  $g$  and  $h$  on a  $64^2$  lattice with parameters  $m_\chi^2 = 0.5$ ,  $\lambda = 0.1$  and  $v = 3$ . We have also observed similar phenomena in  $d = 3$ .

In figure 1 we show nine configuration snapshots of  $\phi$ , each taken after 20,000 lattice updates. These snapshots are taken from a large dataset, which extends from  $g = 0.0$  to

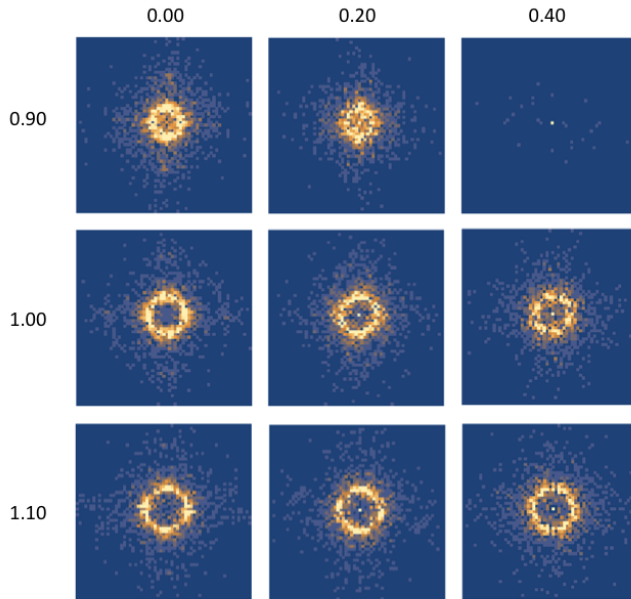


FIG. 2. (color online) The absolute value of the Fourier transforms  $\tilde{\phi}(k)$  for the configurations shown in Fig. 1. We scale each graph so that its colors run from 0 (dark blue) to 10 (light yellow). Any lattice point with magnitude greater than 10 is set to 10. The ring-shaped Fourier transforms correspond to patterning in Fig. 1.

$g = 2.0$  at  $h = 0$  out to  $g$  around 1.0 at  $h = 0.95$ , covering the region where pattern formation occurs. For smaller values of  $g$ , the length scale of pattern formation is too large for a  $64^2$  lattice to reveal much information. For larger values of  $g$ , the length scale of pattern formation is on the order of the lattice spacing so the details of any pattern formation are lost.

In figure 1, we see long line segments, often called *stripes*, at  $h = 0$  and intermediate values of  $g$ . For a given pair of  $g$  and  $h$  values, the width of these stripes is fairly uniform, but there is considerable randomness in the overall pattern. As  $h$  increases, the typical line segment length decreases until commensurate with the width, forming a *dot*. As  $h$  increases beyond this point, the dots shrink until they disappear at the boundary of the pattern-forming region. The variation in pattern morphologies is smooth, as is the change in histograms of  $\phi$  values.

Figure 2 shows the absolute value  $|\tilde{\phi}|$  of the Fourier transforms of the configurations  $\phi$  shown in figure 1. All graphs use the same color scale, but large values were clipped to

a maximum value of 10. This is necessary because as  $h$  increases, the zero mode  $|\tilde{\phi}(0)|$ , representing the expected value of  $\phi$ , would otherwise dominate. The eight patterned configurations have an obvious common feature: a ring in momentum space. The radius of the ring increases with  $g$  but is not heavily dependent on  $h$ . There is no ring at  $(h = 0.4, g = 0.9)$ , but  $|\tilde{\phi}(0)|$  is large, which represents a nonzero expectation value and the absence of patterns.

Much of the literature on pattern-forming models has been based on the idea of microphases. In this approach, patterns are conceptualized in terms of nontrivial, high symmetry solutions of the equations of motion such as stripes, dots or tubes. Solutions of the classical equations with different symmetries are said to represent different microphases. Minimization of  $S$  among different solutions typically suggests a first-order transition between different microphases. In our simulations, we see no evidence for the existence of distinct microphases, nor for thermodynamic transitions between different morphologies. Instead we see a smooth transition between long line segments to shorter ones as  $h$  increases, with a distribution of shapes in each configuration. The average action  $\langle S \rangle$  varies smoothly as  $h$  and  $g$  are varied. In most of the two-dimensional simulations, we see a fairly complete ring in momentum space, consistent with pattern formation without preferred directions. In some cases, however, a smaller number of modes on the ring are excited, and the absence of isotropy is evident in the configurations. This may be related to finite size effects or to locking into an atypical but long-lived pattern. For many systems, it is known that the energy is minimized by regular patterns, typically stripes [13, 14].

Our model is also amenable to analytical treatment. Because  $\chi$  enters quadratically in the action  $S$ , it can easily be integrated out, yielding a nonlocal effective action of the form

$$S_{\text{eff}} = \sum_x \left[ \frac{1}{2} (\partial_\mu \phi(x))^2 + \lambda (\phi^2 - v^2)^2 + h\phi \right] + \frac{g^2}{2} \sum_{x,y} \phi(x) \Delta(x-y) \phi(y). \quad (4)$$

This model has been extensively studied in the case  $m_\chi = 0$ ; see, *e.g.* [2] and references therein. The  $m_\chi = 0$  is sometimes described in the condensed matter literature as Coulomb frustrated because the extra interaction acts against the ferromagnetic behavior of the  $\phi^4$  model [2, 3, 15]. However, our simulations show that the observed patterning behavior is not tied to the long-range nature of the Coulomb interaction.

We determine the value of the order parameter  $\phi_0$  at tree level by minimizing the potential or equivalently by minimizing the effective potential associated with  $S_{\text{eff}}$ :

$$V_{\text{eff}}(\phi_0) = \lambda (\phi_0^2 - v^2)^2 + g^2 \phi_0^2 / 2m_\chi^2 - h\phi_0. \quad (5)$$

The effect of  $\chi$  on  $\phi_0$  is to restore the symmetric phase  $\phi_0 = 0$  for  $h = 0$  at sufficiently large values of  $g$ . Given our simulation results, the details of the phase structure follow from the inverse  $\phi$  propagator obtained at tree level:

$$G^{-1}(q) = q^2 - 4\lambda v^2 + 12\lambda\phi_0^2 + \frac{g^2}{q^2 + m_\chi^2}. \quad (6)$$

Three different behaviors are possible, depending on the zeros of  $G^{-1}$ . If both zeros occur at  $q^2 < 0$ , then the propagator decays exponentially. If the zeros are complex, they must form a complex conjugate pair and the propagator decays exponentially with sinusoidal modulation. The boundary between these two behaviors is by definition a disorder line [16]. If one or both zeros are real and positive, then the linearized theory predicts that these modes will grow exponentially, indicating that the homogeneous phase is unstable. This is the region where pattern formation occurs. This region is determined by noting that  $G^{-1}(q)$  has a minimum at  $q^2 > 0$  provided  $g > m_\chi^2$ . The propagator has tachyonic modes if the minimum lies below zero, corresponding to  $2g - m_\chi^2 - 4\lambda v^2 + 12\lambda\phi_0^2 < 0$ . The region predicted to have tachyonic modes is in reasonable agreement with the boundaries of the pattern-forming region observed in simulation, subject to the limitations imposed by lattice size and spacing.

Our simulations and complementary analytical studies point to a common origin for patterning. The observed ring in Fourier space appears independently of the particular morphology of the configuration in real space. Combined with the gradual transition between different morphologies, this suggests that all pattern-forming behavior is associated with tachyonic modes. We see no indication of a first- or second-order thermodynamic phase transition between supposed microphases. It is of course possible that some currently unknown operator might serve as an order parameter for what are referred to as geometric transitions associated with percolative behavior. It is known in the case of the d=1 Ising model that there is an infinite class of nonlocal string operators, each with its own disorder line. This is associated with the behavior of the model in an imaginary magnetic field, which is the prototypical  $\mathcal{PT}$ -symmetric problem [17], so it is plausible that such behavior may exist in other  $\mathcal{PT}$ -symmetric models.

As a first step towards approximating the behavior of the equilibrium patterning state, we consider a simple model that provides additional insight into the transition between

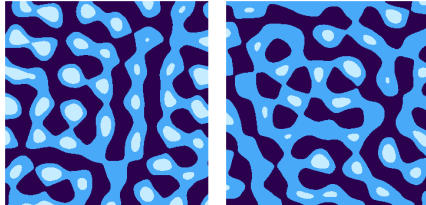


FIG. 3. (color online) Topography of synthetic configurations of the form Eq. (5), for two different sets of  $(k_j, \delta_j)$  and  $\phi_0 = 0$ . The light blue, turquoise, and dark blue regions correspond to the regions where  $\phi(x) > 4$ , where  $0 < \phi(x) < 4$ , and where  $\phi(x) < 0$ , respectively. (This is equivalent to plotting the regions of  $\phi(x)$  that are positive when  $\phi_0 = -4$  or 0.) The synthetic model topography mimics the patterns in the figure 1 field configurations: the light blue region forms a set of droplets, and the turquoise region looks like a striped configuration.

different patterning behaviors. We consider configurations of the form

$$\phi(x) = \phi_0 + \sum_{j=1}^n A \cos(k_j \cdot x - \delta_j) \quad (7)$$

where the momenta  $k_j$  are constant in magnitude but uniformly distributed in direction; the phases  $\delta_j$  are also uniformly distributed. Fig. 3 shows the topography of two configurations with different sets of  $k_j$  and  $\delta_j$  values. Mapping the three topographical contours is equivalent to picking two different values of  $\phi_0$  and coloring each point based on the sign of  $\phi(x)$  for each choice  $\phi_0$ . This rather simple approach reproduces much of the observed pattern morphology. It is clear that any configuration with the structure of Eq. (7) will tend to produce topographic contours that appropriately mimic the patterns of stripes and droplets. It does not, however, reproduce the two-peaked distribution of  $\phi(x)$  values obtained in simulations. Reproducing all aspects of a patterned configuration is a difficult nonlinear problem.

The patterning we observe in simulations is strikingly similar to that in phase transition dynamics, although it is associated with equilibrium behavior. The dynamics of  $\phi$  can be modeled by a Langevin equation

$$\frac{\partial \phi(x)}{\partial t} = -\Gamma \frac{\delta S_{\text{eff}}}{\delta \phi(x)} + \eta(x). \quad (8)$$

where as usual  $\Gamma$  is a decay constant and  $\eta(x)$  is a white noise term. The difference between this model and a standard  $\phi^4$  field theory is the nonlocal term in  $S_{\text{eff}}$  induced by  $\chi$ , which

stabilizes  $\langle\phi\rangle$  in what would otherwise be an unstable region of the phase diagram. It is easy to show that the dynamics of pattern formation have the same enhanced modes in momentum space as the equilibrated configurations do. The dichotomy between a tachyonic origin of patterned phases and the microphase model is reminiscent of the distinction between spinodal decomposition and nucleation and growth in phase transition dynamics. Spinodal decomposition is the mechanism by which unstable states equilibrate while nucleation and growth is associated with the decay of metastable states. We now know [18–20] that there is typically no sharp boundary between these two mechanisms in phase transition dynamics. Because of the close connection between dynamics and statics in this model, we propose that the relation of our tachyonic picture to the microphase picture is essentially the same as that of spinodal decomposition to nucleation and growth.

We now demonstrate that multicomponent  $\mathcal{PT}$ -symmetric scalar field theories with complex actions form a natural class of models associated with pattern formation. Consider a general field theory of this class in  $d$  dimensions where both  $\phi$  and  $\chi$  may have more than one component. The action has the form given by Eq. (1), but with  $V(\phi, \chi)$  an arbitrary potential satisfying the  $\mathcal{PT}$  symmetry condition. As before, we find homogeneous equilibrium phases by minimizing  $V$ , with  $(\phi_0, \chi_0)$  the global minimum. We assume that  $\mathcal{PT}$  symmetry is maintained, which implies that  $\phi_0$  is real,  $\chi_0$  is imaginary and  $V(\phi_0, \chi_0)$  is real. The one-loop effective potential  $V_{\text{eff}}(\phi, \chi)$  is given by

$$V_{\text{eff}}(\phi, \chi) = V(\phi, \chi) + \frac{1}{2} \int \frac{d^d q}{(2\pi)^d} \left[ \log \det (q^2 + \mathcal{M}) \right], \quad (9)$$

where the mass matrix  $\mathcal{M}$  in block form is given by

$$\mathcal{M} = \begin{pmatrix} \frac{\partial^2 V}{\partial \phi^2} & \frac{\partial^2 V}{\partial \phi \partial \chi} \\ \frac{\partial^2 V}{\partial \phi \partial \chi} & \frac{\partial^2 V}{\partial \chi^2} \end{pmatrix}. \quad (10)$$

This mass matrix evaluated at  $(\phi_0, \chi_0)$  is not necessarily Hermitian but is  $\mathcal{PT}$ -symmetric. In the two-component case, we have

$$M = \sigma_3 M^* \sigma_3. \quad (11)$$

This generalizes to the multicomponent case as

$$M = \Sigma M^* \Sigma, \quad (12)$$

where  $\Sigma$  is a diagonal matrix with entries  $\pm 1$ . The characteristic equations for  $M$  and  $M^*$  are the same, so they have the same eigenvalues. As a consequence, the eigenvalues of  $\mathcal{M}$  are either both real or form a complex conjugate pair.

We calculate the one-loop contribution to  $V_{\text{eff}}$  at the tree-level minimum  $(\phi_0, \chi_0)$ . We see easily that  $\det(q^2 + \mathcal{M})$  can be negative if and only if one or more of the eigenvalues of  $\mathcal{M}$  are real and negative. If one or more eigenvalues are negative, then  $V_{\text{eff}}$  will have an imaginary part, indicating instability of the homogeneous phase, and the equilibrium phase is inhomogeneous. The decay rate of the homogeneous phase is [21]

$$\Gamma = \frac{\pi}{2} \int_{\mathcal{R}} \frac{d^d q}{(2\pi)^d}, \quad (13)$$

where  $\mathcal{R}$  is the region of  $q$  space where  $\det \mathcal{M} < 0$ . Note that this decay rate is perturbative, representing a fast decay, in contrast to the slow modes associated with changing pattern morphology. This indicates that relaxation from a given initial condition takes little simulation time relative to autocorrelation time. Adequately sampling the equilibrium state may require a great deal of time depending on the target observables. Note that in the general case, there may be more than one homogeneous solution which is unstable to pattern formation. We cannot necessarily predict which inhomogeneous phase has the lowest free energy. In the case of a theory with three or more components, pattern formation may be quite complicated [13, 14].

The observation of pattern formation in field theories with complex actions raises interesting issues about computational complexity in bosonic models with sign problems. Some of the characteristics observed in our simulations, such as large numbers of metastable configurations and very slow quasizero modes, are reminiscent of glassy behavior. It is known that the problem of finding the ground state of an Ising model with general couplings is NP-hard [22]. Certain fermionic models with sign problems have been mapped to the Ising spin glass, a known NP-hard problem [23]. In the pattern-forming region of the model studied here, the computational complexity, as measured by our ability to adequately sample equilibrium behavior, increases dramatically; this is similar to the behavior of a spin glass, but without the random character of spin glass interactions. In PT-symmetric scalar field theories, imaginary couplings can change the fundamental behavior of interactions, making attractive couplings repulsive. This in turn can set up a conflict between attractive and repulsive forces, a well-known cause of pattern formation. For example, nuclear pasta, believed

to occur in neutron star crusts, arises from the attractive nuclear force and the repulsive Coulomb force [11]. Thus the connection between the sign problem and pattern formation is in hindsight natural.

Our original interest in field theories with sign problems was motivated by QCD at finite density, a multi-component field theory with a generalized  $\mathcal{PT}$  symmetry. The widely-conjectured phase structure of finite density QCD is characterized by a first-order line with a critical end point in the  $Z(2)$  universality class, similar to the model studied here. This raises the interesting possibility that finite-density QCD might exhibit pattern formation around its critical end point, composed of regions of confined and deconfined phase. As discussed above, patterns may also form out of equilibrium, an interesting feature from an experimental point of view.

## Acknowledgements

MCO thanks C. M. Bender and Z. Nussinov and STS thanks A. Grebe and G. Kanwar for helpful discussions. STS was supported by the NSF Graduate Research Fellowship and the MIT Physics Department Peskoff Fellowship.

---

\* leandro.medina.lv@gmail.com

† mco@wustl.edu

‡ schindler@wustl.edu

§ stellas@mit.edu

- [1] Michael Seul and David Andelman. Domain shapes and patterns: The phenomenology of modulated phases. *Science*, 267(5197):476–483, 1995. doi:10.1126/science.267.5197.476.
- [2] C. B. Muratov. Theory of domain patterns in systems with long-range interactions of coulomb type. *Phys. Rev. E*, 66:066108, Dec 2002. doi:10.1103/PhysRevE.66.066108.
- [3] C. Ortix, J. Lorenzana, and C. Di Castro. Coulomb-frustrated phase separation phase diagram in systems with short-range negative compressibility. *Phys. Rev. Lett.*, 100:246402, Jun 2008. doi:10.1103/PhysRevLett.100.246402.

- [4] Konrad Osterwalder and Robert Schrader. Axioms for euclidean green's functions. *Communications in Mathematical Physics*, 31(2):83–112, Jun 1973.
- [5] Carl M. Bender and Stefan Boettcher. Real spectra in non-Hermitian Hamiltonians having PT symmetry. *Phys. Rev. Lett.*, 80:5243–5246, 1998. doi:10.1103/PhysRevLett.80.5243.
- [6] Carl M. Bender. Making sense of non-Hermitian Hamiltonians. *Rept. Prog. Phys.*, 70:947, 2007. doi:10.1088/0034-4885/70/6/R03.
- [7] M. E. Fisher. Yang-Lee Edge Singularity and  $\phi^3$  Field Theory. *Phys. Rev. Lett.*, 40:1610–1613, 1978. doi:10.1103/PhysRevLett.40.1610.
- [8] Peter N. Meisinger and Michael C. Ogilvie. PT Symmetry in Classical and Quantum Statistical Mechanics. *Phil. Trans. Roy. Soc. Lond.*, A371:20120058, 2013. doi:10.1098/rsta.2012.0058.
- [9] Philippe de Forcrand. Simulating QCD at finite density. *PoS*, LAT2009:010, 2009. doi:10.22323/1.091.0010.
- [10] Sourendu Gupta. QCD at finite density. *PoS*, LATTICE2010:007, 2010. doi:10.22323/1.105.0007.
- [11] D. G. Ravenhall, C. J. Pethick, and J. R. Wilson. Structure of Matter Below Nuclear Saturation Density. *Phys. Rev. Lett.*, 50:2066–2069, 1983. doi:10.1103/PhysRevLett.50.2066.
- [12] Michael C. Ogilvie and Leandro Medina. Simulation of Scalar Field Theories with Complex Actions. *PoS*, LATTICE2018:157, 2018. doi:10.22323/1.334.0157.
- [13] Zohar Nussinov.  $O(n)$  spin systems, some general properties: A Generalized Mermin-Wagner-Coleman theorem, ground states, Peierls bounds, and dynamics. 2001.
- [14] Saurish Chakrabarty and Zohar Nussinov. Modulation and correlation lengths in systems with competing interactions. *Phys. Rev. B*, 84:144402, Oct 2011. doi:10.1103/PhysRevB.84.144402.
- [15] C. Ortix, J. Lorenzana, and C. Di Castro. Universality classes for coulomb frustrated phase separation. *Physica B: Condensed Matter*, 404(3):499 – 502, 2009. doi:https://doi.org/10.1016/j.physb.2008.11.045.
- [16] John Stephenson. Ising model with antiferromagnetic next-nearest-neighbor coupling: Spin correlations and disorder points. *Phys. Rev. B*, 1:4405–4409, Jun 1970. doi:10.1103/PhysRevB.1.4405.
- [17] P. N. Timonin and Gennady Y. Chitov. Infinite cascades of phase transitions in the classical ising chain. *Phys. Rev. E*, 96:062123, Dec 2017. doi:10.1103/PhysRevE.96.062123.

- [18] J. S. Langer, M. Bar-on, and Harold D. Miller. New computational method in the theory of spinodal decomposition. *Phys. Rev. A*, 11:1417–1429, Apr 1975. doi:10.1103/PhysRevA.11.1417.
- [19] K. Binder, C. Billotet, and P. Miold. On the theory of spinodal decomposition in solid and liquid binary mixtures. *Zeitschrift für Physik B Condensed Matter*, 30(2):183–195, Jun 1978.
- [20] Amitabha Chakrabarti. Transition from metastability to instability in the dynamics of phase separation. *Phys. Rev. B*, 45:9620–9625, May 1992. doi:10.1103/PhysRevB.45.9620.
- [21] Erick J. Weinberg and Ai-qun Wu. Understanding Complex Perturbative Effective Potentials. *Phys. Rev.*, D36:2474, 1987. doi:10.1103/PhysRevD.36.2474.
- [22] F Barahona. On the computational complexity of ising spin glass models. *Journal of Physics A: Mathematical and General*, 15(10):3241–3253, oct 1982. doi:10.1088/0305-4470/15/10/028.
- [23] Matthias Troyer and Uwe-Jens Wiese. Computational complexity and fundamental limitations to fermionic quantum monte carlo simulations. *Phys. Rev. Lett.*, 94:170201, May 2005. doi:10.1103/PhysRevLett.94.170201.